Changing Idling Behavior Through Dynamic Idle Detection and Air Quality Messaging

Tristalee Mangin, Xiwen Li, Saba Mahmoudi, Rehman Mohammed, Nathan Page, Sara Peck, Ashton Snelgrove, *Senior Member, IEEE*, Evan Blanchard, Dillon Tang, Lizzie Pinegar, Owen Leishman, J. Nicholas Rice, Gregory Madden, Pierre-Emmanuel Gaillardon, *Senior Member, IEEE*, Ross Whitaker, and Kerry Kelly

***Abstract*—Air quality impacts on human health are an increasing concern globally. Vehicle pollution is a particular concern because of its multiple adverse health effects, and discretionary vehicle idling contributes significantly to local-scale poor air quality. This study introduces a novel approach to traditional static (unchanging) anti-idling signage. Here, we demonstrate a system, called SmartAir, that provides dynamic social-norm messages to drivers coupled with information about idling status or vehicle emissions in the area. A machine learning algorithm with audio and video inputs determines vehicle idling status. Vehicle emissions are measured using a suite of low-cost air quality nodes. In this study, we show that the SmartAir system reduces idling time by 28.0% and local CO_2 concentrations by 29.5% compared with background.**

***Index Terms*—Anti-idling, automated vehicle idling detection, dynamic feedback, IoT, low-cost vehicle emission monitoring, sensor network, smart cities, social-norm messaging.**

I. Introduction

In THE United States, transportation is one of the greatest sources of air pollution [1], and poor air quality negatively affects human health and healthcare costs [2], [3]. Vehicle pollution can negatively impact various medical conditions, from cognitive function in children [4] to lung and respiratory function in adults and children [5], [6], [7]. In addition, greenhouse gases are emitted during engine idling, with 30 million tons of CO_2 generated from personal vehicle idling alone [8].

Individual choices can significantly affect community- and individual-level air quality. As the urban population grows, behavior patterns become increasingly important. Locations where idling vehicles congregate, such as schools and hospital drop-off and pickup zones, are prime examples of where individual choices can dramatically affect hyperlocal air quality [9]. Entering these zones means passing through microclimates of elevated pollution, including $PM_{2.5}$ (particles smaller than 2.5-μm diameter), carbon monoxide (CO), carbon dioxide (CO_2), volatile organic compounds (VOCs), ozone (O_3), and oxides of nitrogen (NO_x) [6], [10]. Children and individuals in wheelchairs are particularly vulnerable to vehicle exhaust because of their breathing height; they can experience up to 60% higher levels of pollution ($PM_{2.5}$) compared with standing adults [7], [11].

Behavior change is a promising strategy to reduce idling [12], [13]. However, anti-idling signage and education have, at best, a mixed record of success [9], [14], [15], [16], [17]. A different approach—dynamic feedback with digital speed displays—effectively influences driver behavior (reduces speeding) and reduces traffic accidents [18], [19], [20], [21]. Long-term evaluations indicate that digital speed displays are effective for as long as they are in place [22], [23]. The theoretical basis for the efficacy of dynamic speed displays is that public displays of a social-norm violation (i.e., speeding) could be reputationally harmful [24], [25]. Those currently, or about to, violate this norm often reduce their speed to avoid these reputational consequences (e.g., verbal confrontation, gossip, and social ostracization [26], [27], [28], [29], [30]). Mahmoudi et al. [31] reported that when drivers read an injunctive social-norm message hypothetically presented in a drop-off/pickup zone at a school, the duration of their intent-to-idle significantly decreases. Adding an image of an idling vehicle, exhaust, and a child further reduces idling by 41.9%.

IoT-based low-cost air quality sensor networks have become an increasingly popular method for understanding neighborhood-scale differences in air quality, wildfire smoke plumes, indoor air quality, and individual pollution exposure [32], [33], [34], [35], [36], [37], [38], [39]. Fewer studies have applied these low-cost sensor networks to mobile emissions [40], [41]. Even fewer studies have used IoT sensors

Received 17 May 2025; revised 8 August 2025; accepted 17 September 2025. Date of publication 22 September 2025; date of current version 20 November 2025. This work was supported in part by the National Science Foundation; in part by the Smart and Connected Communities Integrative Research Grants (SCC-IRG) TRACK 2: SmartAir: Informing Driving Behavior Through Dynamic Air-Quality Sensing and Smart Messaging under Grant 1952008; in part by Utah Clean Air Partnership (UCAIR); and in part by Chevron, Salt Lake City. *(Corresponding author: Tristalee Mangin.)*

Tristalee Mangin, Evan Blanchard, Dillon Tang, and Kerry Kelly are with the Department of Chemical Engineering, University of Utah, Salt Lake City, UT 84112 USA (e-mail: tristalee.mangin@utah.edu).

Xiwen Li, Rehman Mohammed, and Ross Whitaker are with the Kahlert School of Computing, University of Utah, Salt Lake City, UT 84112 USA.

Saba Mahmoudi and Gregory Madden are with the Department of Psychology, Utah State University, Logan, UT 84322 USA.

Nathan Page, Ashton Snelgrove, Owen Leishman, and Pierre-Emmanuel Gaillardon are with the Department of Electrical and Computer Engineering, University of Utah, Salt Lake City, UT 84112 USA.

Sara Peck is with the Department of Psychology, Western New England University, Springfield, MA 01119 USA.

Lizzie Pinegar is with the Department of Chemical Engineering and Atmospheric Science, University of Utah, Salt Lake City, UT 84112 USA.

J. Nicholas Rice is with the Industrial Hygiene, Intermountain Health, Salt Lake City, UT 84143 USA.

This article has supplementary downloadable material available at https://doi.org/10.1109/JIOT.2025.3612853, provided by the authors.

Digital Object Identifier 10.1109/JIOT.2025.3612853

to influence driver behavior. A notable exception is Farrag et al. [42], who developed an IoT-based vehicle emission monitoring system to notify drivers when tailpipe emissions exceed acceptable levels, although they did not report the system's impact on vehicle emissions or a driver's decision to repair the vehicle.

The goal of this project is to evaluate the effects of the social-norm approach on idling behavior by using an IoT-based dynamic message to communicate near real-time information about idling vehicles and hyperlocal air quality. This dynamic feedback system is called the SmartAir System.

II. Background

Anti-idling campaigns typically rely on static signage, letters, fact sheets, and education [9], [43], [44], [45]. Two studies, Mendoza et al. [44] and Ryan et al. [9], found anti-idling campaigns based on the EPA's Idle-Free Schools Toolkit at elementary schools. Mendoza et al. [44] showed an 11% reduction in idling vehicles obtained from vehicle counts precampaign and postcampaign. Ryan et al. [9] found a 75.9% decrease in $PM_{2.5}$ concentration and a 62.5% decrease in elemental carbon concentration, measured with Harvard-type $PM_{2.5}$ impactor.

Sharma et al. [43] showed a 14% reduction in estimated CO_2 emissions after a 40-day awareness campaign at signalized intersections in Delhi (from 9357 CO_2 equivalent tons/day to 7976 tons/day). The anti-idling campaign by Rumchev et al. [45] shows a decreased number of idling vehicles in eight out of ten schools using onsite signage, newsletters, and fact sheets. Of particular interest, Abrams et al. [46] demonstrated the effectiveness of social-norm persuasive messaging on idling, reporting a 42% increase in the number of drivers who turned off their engines in response to anti-idling signage posted near a railway crossing in U.K., compared with the baseline.

To the best of the authors' knowledge, aside from the vehicle idling detection algorithm employed in this study [47], only one other study by Bastan et al. [48] reported the automatic detection of idling vehicles, and they used deep neural networks and infrared imaging.

III. SmartAir System

This section discusses the components of the SmartAir system and how they interact. Section IV, provides information about the field deployment.

A. Overall System Structure

Fig. 1 shows the structure of the SmartAir system, which integrates audio, video, and air quality information to provide near real-time updates about either vehicle idling status or air quality levels. This information is displayed as a message and accompanying image on large outdoor monitors that drivers in the target area can view (messages discussed in Section IV-B).

B. Server

A desktop computer (Windows OS) and a router (TP-Link Archer C7 AC1750) are configured to establish a standalone wireless network. The Mosquitto broker for Windows facilitates MQTT communication between the air quality sensor nodes and the computer. Multithreaded Python programs manage network operations, MQTT data handling, web server functionality, and the machine learning-based idle detection algorithm. In addition, the system saves all collected data on the computer's disk for further analysis. This setup will be referred to as the server throughout the rest of this article.

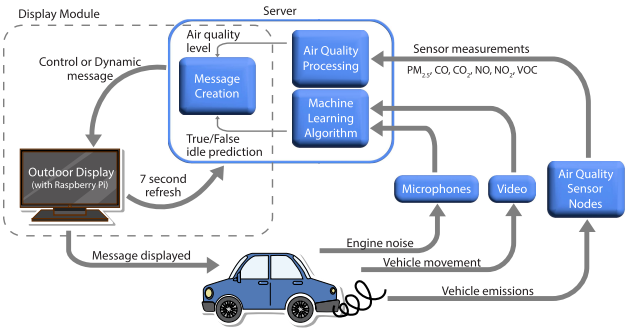

Fig. 1. Overview of the SmartAir System.

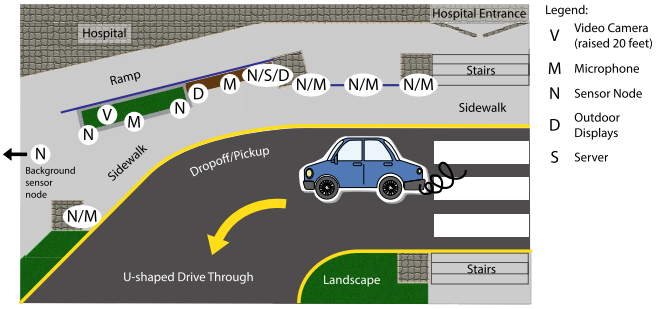

Fig. 2. Overview of the hospital deployment site drop-off/pickup zone. About five and six vehicles could fit end-to-end in the sampling area. The driving lane is two vehicles wide.

C. Audio Nodes and Video Monitor

We utilize six off-the-shelf microphones (three sets of Rode GO II Dual Channel Wireless Systems, with each set comprising one receiver and two transmitters) and a webcam (EMEET 1080P) for audio and video acquisition (see Fig. 2). Each transmitter captures audio signals and transmits them wirelessly to the receiver. The receiver, connected to the server via a USB cable, converts the incoming audio signals to a digital format and transfers them to the computer. The webcam is connected to the computer using a USB repeater cable, which is continuously charged during operation to prevent lag. The camera is set to 25 f/s (40 ms for each new frame), and the audio and video transmission times are 5 and 15 ms, respectively. To minimize audio and video loss in case of system interruptions, we save the recordings every hour and start a new recording. This process results in a recording gap that lasts on average 2 min every hour.

D. Idle Detection

We employ a deep learning algorithm that processes audio, video, and user inputs to detect idling vehicles, as detailed in [47]. This algorithm identifies stationary vehicles that produce sound and operates in three distinct stages. In the first stage, our motion-detection model predicts a bounding box and motion status of each vehicle in the scene. In the second stage, for each stationary vehicle, the algorithm identifies

the nearest microphone using microphone pixel coordinates (provided manually by the user at the beginning of each day) along with the predicted bounding boxes. It then retrieves the corresponding audio signal from the nearest microphone. In the third stage, an audio classifier analyzes the retrieved audio and determines whether it detects engine noise. Next, the system consolidates all information, generates vehicle idling status predictions, and writes the results to an output file at 1-s intervals for the display module (see Section III-F). The algorithm requires 10 ms/frame. Therefore, each vehicle idling status prediction is at most 65 ms (55 ms for the audio and video acquisition and 10 ms for the algorithm).

To address challenging scenarios such as overlapping vehicles, background noise, and moving cars—beyond the simple case of a single vehicle—Li et al. [47] proposed a machine learning framework that incorporates four key techniques.

1) *Unidirectional Microphones*: The system employs unidirectional microphones, which capture sound primarily from a specific direction while attenuating signals from other directions, thereby reducing background noise.
2) *Nearest Microphone Matching*: For each static vehicle, the system identifies the nearest microphone. Combined with large intermicrophone spacing and the directional sensitivity of the microphones, this allows the system to focus on the acoustic signal of the target vehicle.
3) *Contrastive Audio Representation Learning*: The audio classifier is trained using supervised contrastive learning to construct a latent space where sounds of the same category cluster together while dissimilar sounds are pushed apart. This enables the model to better distinguish between different types of car engine sounds and unrelated background sounds (e.g., human speech).
4) *Prediction Label Smoothing*: During deployment, the system checks all predictions in the last second and chooses the one that appears most frequently, helping to smooth out occasional misclassifications.

Together, these four components along with the simple overall idle status message for the display, make the system relatively robust in complex multivehicle environments.

E. Air Quality Node

The SmartAir system includes eight air quality nodes, with seven sampling nodes and one background node (see Fig. 2). Each node employs an ESP32 microcontroller. It is USB-powered and uses Wi-Fi to connect to the server. Each node contains the following measurements: temperature and humidity (Texas Instruments HDC1080), $PM_{2.5}$ (Plantower PMS3003), CO_2 (Senseair K30 FR), CO (Alphasense CO-B4), NO (Alphasense NO-B4), NO_2 (Alphasense NO2-B43F), and tVOC (Alphasense PID-AH). Sensor measurements are collected at 1-s intervals, saved to an onboard SD card, and published to the MQTT broker. The published messages average 700 bytes and require approximately 5 ms to transmit from publisher to subscriber using the MQTT broker with quality of service set to 0 (the fastest MQTT setting). The server saves messages received from the air quality sensor nodes as JSON files in a local data directory (700-byte JSON messages write to the directory in less than 1 ms).

Radio frequency interference between the microphones and the air quality nodes caused frequent disconnections of the air quality nodes when operated simultaneously. Therefore, we developed two separate dynamic messages, one based on the idle status and the other on air quality measurements (see Section IV-B). The SD card on the sampling air quality nodes stores sensor measurements on days when the idle status message is operating. The background air quality node always stores measurements on the SD card, since the distance to the server prohibits wireless transmission of the measurements. Otherwise, the computer processes incoming sensor measurements and uses the CO_2 sensor measurement as a proxy for vehicle emissions. CO_2 measurements tend to be the most consistent indicator of vehicle emissions [49]. The maximum CO_2 measurement from the sensors is scaled to a value between 0 and 100 based on a concentration range from preliminary field tests (380–440-ppm uncorrected CO_2 concentration, note: K30 FR measurements are biased low and corrections are applied postdeployment), with anything less than or greater than the range mapping to 0 and 100, respectively. The scaled CO_2 is written to an output file available to the display module (see Section III-F) at 1-s intervals (Python processing and file writing takes less than 1 ms).

This article only presents CO_2 measurements due to space limitations and because CO_2 is a key indicator of idling emissions [49]. A total of 12 CO_2 sensors were calibrated in the laboratory with a concentration-only linear regression compared with a TSI Q-Track 7575 with probe 982, and they exhibited low sensor-to-sensor variability, with a coefficient of variation (CV) of 2.49% in the slopes. This CV is substantially lower than the EPA's <30% CV recommendation for low-cost sensors [50], [51]. In addition, CO_2 sensor measurements are corrected using a multiple linear regression model developed from laboratory experiments in an environmental chamber controlling concentration, temperature, and relative humidity. A follow-up publication will report the sensor laboratory performance, correction factors, and complete field deployment air quality results. It is worth noting that this article focuses on relative changes in air quality metrics rather than absolute concentrations (see Section IV-C).

F. Display Module

Two Raspberry Pi devices (Raspberry Pi 4 Model B) with Chromium browsers serve as clients for the web server. Each Raspberry Pi is connected to a 55-in LG outdoor digital display (LG 55XS4J-B) and uses Wi-Fi to link to the server. Upon start-up, a bash script launches the browser, automatically directing it to an index HTML file hosted on the server. The index file redirects requests to the appropriate daily message HTML file. Section IV-A details each day and message type: control, dynamic idle status, and dynamic vehicle emission meter. Section IV-B contains details on message development. Messages are implemented using HTML, CSS, and JavaScript.

A 7-s loop between messages was selected to allow drivers reading at a fifth grade level or above [52] to read the messages while navigating through traffic in the drop-off/pickup zone. The most recent idle status prediction or scaled CO_2

TABLE I
DEPLOYMENT DATES, MESSAGE, AND SUMMARY INFORMATION

Date	Day of Week	Message	N_V[1,2]	N_I[1,3]	t_T (min)[1]	t_V (min)[4]	t_I (min)[1]	T_{max} (F)[5]	T_{avg} (F)[5]	RH_{avg} (%)[5]
28-Jul-23	Friday	Control	74	75	206.8	123.5	86.0	102	87	23
1-Aug-23	Tuesday	Control	69	60	233.6	195.7	73.5	91	81	42
2-Aug-23	Wednesday	Idle Status	66	67	202.3	170.3	47.6	78	71	84
3-Aug-23	Thursday	Vehicle Emission Meter	63	75	226.0	176.3	56.8	83	73	74
4-Aug-23	Friday	Control	60	50	241.6	107.0	60.8	86	74	54
7-Aug-23	Monday	Idle Status	58	53	243.5	129.0	34.3	88	77	41
8-Aug-23	Tuesday	Vehicle Emission Meter	67	62	243.5	183.6	33.4	82	73	43
9-Aug-23	Wednesday	Control	80	48	243.5	172.6	53.0	88	76	34
10-Aug-23	Thursday	Vehicle Emission Meter	61	45	268.3	190.5	45.5	94	83	29
11-Aug-23	Friday	Idle Status	64	82	242.3	159.9	65.2	93	83	38
14-Aug-23	Monday	Control	68	71	243.0	153.9	93.4	95	80	32
15-Aug-23	Tuesday	Vehicle Emission Meter	78	64	243.7	151.2	64.7	97	85	33
16-Aug-23	Wednesday	Idle Status	77	74	243.4	172.6	57.0	96	84	39
17-Aug-23	Thursday	Idle Status	96	113	233.2	181.6	70.1	98	86	47
18-Aug-23	Friday	Vehicle Emission Meter	81	66	242.7	158.1	66.8	94	85	40

Where N_V is the number of vehicles, N_I is the number of idling events, t_T is the total sampling time, t_V is the time with vehicles in the drop-off/pick-up zone, t_I is the time with idling vehicles in the drop-off/pick-up zone, T_{max} is the maximum daily temperature, T_{avg} is the average daily temperature, and RH_{avg} is the average daily relative humidity.
[1]Based on notes taken continuously by onsite personnel.
[2]Any vehicle that entered the drop-off/pick-up zone (passed through or stopped).
[3]A single vehicle can have multiple idling events. Therefore, the number of idling events can be greater than the number of vehicles.
[4]Based on the vehicles detected in the frame from the video model machine learning algorithm.
[5]Temperature and relative humidity from the Salt Lake City International Airport, UT US WBAN:24127 (ICAO:KSLC) station [54].

concentration is used for the update since these values are generated faster than the message loop interval. Caching is disabled to support frequent updates. Web server transmission and JavaScript processing complete in about 10 ms. The total latency from data generation to display is at most 75 ms (65 ms for idle status predictions or 7 ms for scaled CO_2 values, plus 10 ms for message generation) which is far less than the 7-s loop time.

IV. FIELD DEPLOYMENT

A. Site Description and Experimental Design

We evaluate the SmartAir System at Intermountain Health LDS Hospital in Salt Lake City, UT, USA (40.77860, −111.88032). The system is installed at the hospital's main entrance, which features a U-shaped drop-off/pickup zone beneath a 9.1-m-high ceiling. Fig. 2 depicts the hospital site and identifies the locations of the SmartAir System components.

To ensure stable and clear microphone signal acquisition, the six microphone transmitters are placed 2–3 m from the curb and spaced 2-m apart along the wall adjacent to drop-off/pickup zone (see Fig. 2). The inverse-square law predicts a 10-dB drop in engine sound pressure level when microphones are placed 10 m from an on-road vehicle, pushing the signal close to ambient levels [53]. For video recording, we mount a webcam on top of a 6.1-m tripod positioned to provide a full view of the sampling area (see Fig. 2).

Like the microphones, we deploy seven air quality nodes 2–3 m from the curb, spaced about 1.7 m apart in the drop-off/pickup zone (see Fig. 2). The background air quality node is placed outside the drop-off/pickup zone approximately 15.2 m from any potential vehicle idling.

This evaluation occurred on 15 weekdays, five days for each message, with approximately 4 h of sampling between approximately 11 A.M. and 5 P.M. local time. Table I lists the deployment dates, message type, meteorological data, number of vehicles observed each day and idling time. The three message types are rotated to capture different days of the week and weather conditions.

B. Messages

Section III-F discusses the workflow for displaying the three messages. Fig. 3 shows each message with a wireframe diagram depicting how the messages are updated. The messaging was co-developed with hospital personnel. The dynamic messages [see Fig. 3(b) and (c)] have two parts. The first part is the social-norm statement identifying the desired cultural or behavioral norm [55]. The second part is the information indicating how the individuals are or are not adhering to the norm with the intent of encouraging behavioral change [56].

Predeployment surveys indicated that simpler messages had a greater influence on driver behavior [31]. Therefore, the second part of the dynamic messages is intentionally simple, and shows either the overall idling status in the drop-off/pickup zone [see Fig. 3(b)] or a slider for vehicle emissions [see Fig. 3(c)] measured in the drop-off/pickup zone.

C. Data Analysis

We correct the CO_2 measurements (see Section III-E) and conduct initial screening, which entails removing measurements for a sensor if: the raw signal-to-noise ratio is less than 2 dB [57], [58], they occur within 5 min of cycling the device's power, or they coincide with abnormal periods noted in the field logs. These abnormal periods include: smoking in the sampling area, sprinklers operating, or note takers being overwhelmed or distracted, making field notes unreliable.

Next, the sensor concentration measurements are divided into two datasets: one when no vehicles are present in the drop-off/pickup zone and one when vehicles are present. We use

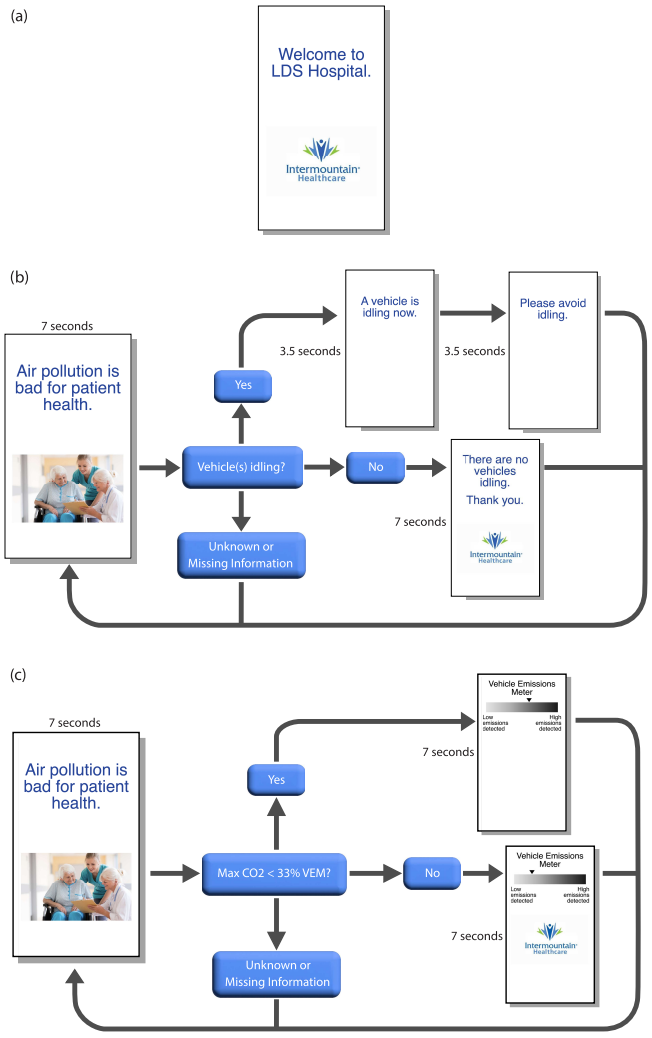

Fig. 3. (a) Static control message. (b) Dynamic social norm plus idling status message. The wireframe shows the transition method and transition times between the first part of the message, the social-norm statement, and the second part of the message, about idling status in the drop-off/pickup zone, provided by a machine learning algorithm. (c) Dynamic social norm plus vehicle emission meter message. The wireframe shows the transition method and transition times between the first part of the message, the social-norm statement, and the second part, about vehicle emissions detected in the drop-off/pickup zone. A scaled CO_2 concentration serves as the proxy for vehicle emissions (see Section III-E).

the no-vehicles-detected dataset to calculate a rolling hourly background CO_2 concentration for each device. We perform a second screening on the vehicles detected dataset by dropping any measurements if the background calculation included fewer than 15 min of measurements (i.e., less than 25% of the hour). We also remove outliers using the z-score method [59], where we define an outlier as any measurement or background value with a z-score greater than 10. This threshold accounts for the expected variability in measurements due to vehicle emissions.

The rolling background concentration (from the no-vehicles-detected dataset) is subtracted from the measured concentration for each sensor, producing a concentration above background value in the vehicles-detected dataset. This value allows for comparison of the messages while minimizing the impacts of intrasensor variability, changes in ambient concentrations, and meteorological conditions.

Finally, driver idling durations and concentrations above background are separated by message type. These data are not normally distributed (idling duration Shapiro–Wilk test, $p < 0.0001$; concentrations above background Anderson–Darling test, $p < 0.0001$), and the concentrations above background exhibit unequal variances (F-test, $p < 0.0001$). Therefore, a Kruskal–Wallis test is used to evaluate whether idling durations or concentrations above background differed by message type. When the Kruskal–Wallis test indicated a significant effect, we conduct post hoc pairwise comparisons using Dunn's test with Bonferroni correction for multiple testing. We consider results statistically significant at $p < 0.05$.

V. Results and Discussion

The supplementary material includes a video of the SmartAir system in operation at the hospital drop-off/pickup zone, showcasing the dynamic idle status message. The video is of the author's personal vehicle, rather than a patient's.

A. Idle Detection Algorithm Performance

The audio and video recording coverage ratio was 90.3% throughout the deployment. Table II provides the idle detection algorithm performance for the no-idling and idling labels. True positive rate (TPR) is the ratio of correctly classified positive labels to all positive labels, using field notes as "ground truth." The average no-idling and idling label TPRs are 96.6% and 78.3%, respectively. From tests conducted prior to the full deployment, Li et al. [47] reported no-idling versus idling detection average precision (AP) as 91.1% and 71.0%, respectively. The AP metrics are computed based on per-vehicle aggregated results, and an AP above 70% generally indicates that the model has a reasonable ability to detect whether each vehicle is idling.

B. Driver Behavior Impacts

The analyses reveal a significant effect of message type ($p < 0.0001$) on idling duration. Fig. 4 shows that the proportion of time in the drop-off/pickup zone that drivers idle is significantly lower (relative to the control message) for both the social-norm plus idling ($p = 0.002$) and social norm plus vehicle emission meter messages ($p < 0.0001$). In addition, the proportion of idling time for the social norm plus vehicle emission meter message is significantly lower than the social norm plus idling message ($p = 0.029$). This study finds an average 28.0% reduction in the proportion of time spent idling when using the dynamic messages compared with the control message (23.3% and 32.7% for the idling and vehicle emission meter messages compared with the control, respectively).

These findings are consistent with the focus theory of normative conduct [55], which holds that drawing attention to expected norms of conduct can change behavior in the direction of the norm. Driven by this theory, the SmartAir display provided a clear injunctive social-norm message—air

TABLE II
IDLE DETECTION ALGORITHM FIELD PERFORMANCE

Date	Day of Week	Message[1]	Deployment Time with Field Validation	No-Idling Label TPR	Idling Label TPR
1-Aug-23	Tuesday	Control	99.9%	96.1%	77.0%
2-Aug-23	Wednesday	Idle Status	96.7%	94.9%	68.0%
4-Aug-23	Friday	Control	98.8%	98.1%	91.0%
7-Aug-23	Monday	Idle Status	96.6%	98.2%	77.8%
9-Aug-23	Wednesday	Control	96.7%	97.7%	68.8%
11-Aug-23	Friday	Idle Status	98.8%	97.1%	77.1%
14-Aug-23	Monday	Control	98.4%	97.2%	80.9%
16-Aug-23	Wednesday	Idle Status	95.0%	94.3%	83.3%
17-Aug-23	Thursday	Idle Status	92.1%	95.5%	80.7%

[1]We run the idle detection algorithm on control message days (except Friday, July 28th) to calculate algorithm field performance even though the control message does not use the output.
TPR - true positive rate.

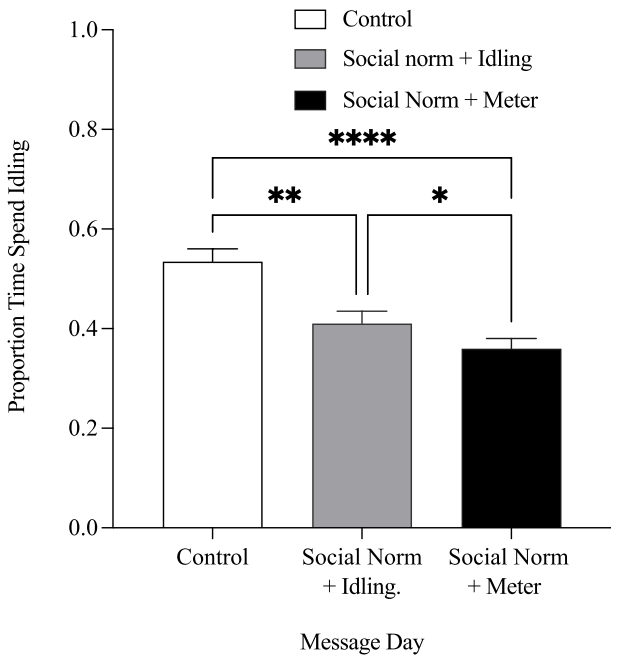

Fig. 4. Driver's proportion of time in the drop-off/pickup zone spent idling for the three messages (control, social norm plus idling status, and social norm plus vehicle emission meter). Note: *p <0.01, **p <0.001, and ****p < 0.0001.

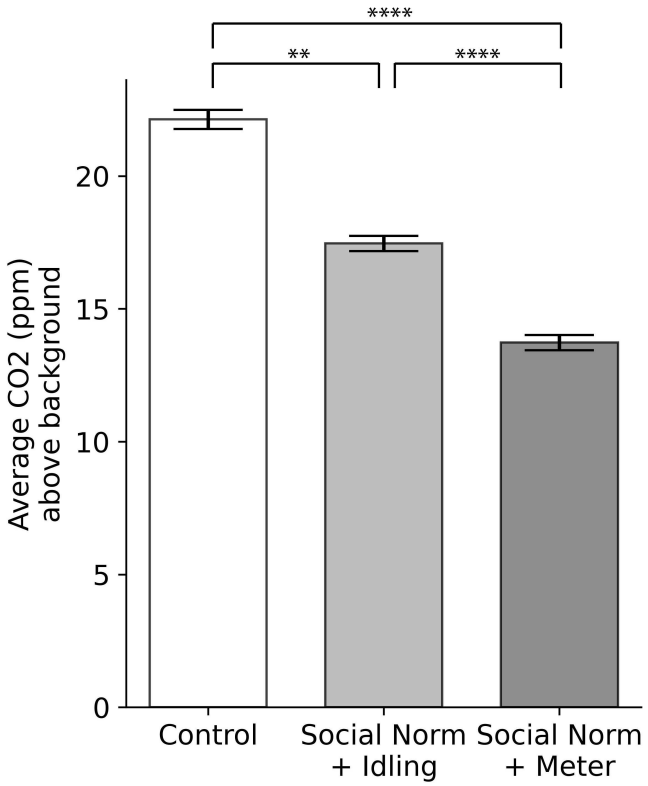

Fig. 5. Average CO_2 concentration above background for each message type (control, social norm plus idling status, and social norm plus vehicle emission meter). The background is device specific (see Section IV-C). Error bars indicate the 95% confidence interval. Note: *p <0.01, **p <0.001, and ****p < 0.0001.

pollution is bad for patient health, please avoid idling. The display may have prompted other drivers to observe social-norm violations and to expect that others were monitoring their idling behavior. This was expected to reduce idling as drivers sought to avoid embarrassment or other negative interpersonal consequences that might occur because of their norm-violating behavior [28], [60]. Our findings are consistent with other studies showing the efficacy of social-norm messaging on driver intent-to-idle [31] and actual idling behavior [46].

C. Air Quality Impacts

The air quality nodes had an average daily data completeness of 99.1%, with values ranging from 95.3% to 99.9%. Fig. 5 shows the comparison of the CO_2 levels for the control message to those for social norm plus idling status and social norm plus vehicle emission messages. The CO_2 concentration above background shows a decrease of 4.7 ppm (21.1%, p <0.001) for the social norm plus idle status message compared with the control message and a decrease of 8.4 ppm (38.0%, p < 0.0001) for the social norm plus vehicle emission meter message compared with the control message. The average concentration decrease for the dynamic

messages compared with the control message is 6.5 ppm (29.5% decrease).

The authors did not identify previous anti-idling studies that directly measured CO_2 concentration. An anti-idling campaign in Canada shows a 33% reduction in estimated CO_2 emissions using the NRCan Gas Emission Calculation Tool [61]. While Sharma et al. [43] showed a 14% reduction in estimated CO_2 emissions, calculated from estimated reductions in fuel consumption and emission factors, after an awareness campaign at signalized intersections in Delhi.

D. Limitations and Future Work

This study has several limitations. The field deployment took place during the summer. We expect seasonality, particularly temperature, to impact human behavior [13], and low-cost sensors are sensitive to ambient temperature and relative humidity changes [62]. Vehicle efficiency, and consequently CO_2 emissions, also change with temperature and vehicle load (air conditioning) [63]. Using low-cost sensors increases the uncertainty of the air quality measurements [62] but provides benefits, including small size, portability, quiet operation, scalability, and cost. We neither measure wind speed or direction for air quality analysis nor do we analyze plume dissipation.

Additional limitations relate to the physical deployment location. The hospital site features a partially covered area that protects equipment from weather and wind and improves display visibility by providing shade. Deploying this system in an unprotected area requires hardening of the equipment for weather and potentially brighter displays. In addition, air quality measurements are impacted by differing plume dissipation characteristics, such as in an open area. This study was limited by its 15-day duration and the deployment of equipment at a single location, which restricts the generalizability of the results.

After the deployment was completed, the authors identified a design issue with the air quality node printed circuit board. The board was supposed to have two voltage buses, one 3.5 V and one 5 V, but a short between the buses resulted in a single approximately 4-V bus. The Senseair K30 FR CO_2 sensor calls for a 4.5–14 VDC supply [64]. However, Senseair technical support suggests that if the sensor provided a signal, it had sufficient power. In addition, we ran the concentration-only laboratory test again for some K30 FR sensors (see Section III-E) using the 4-V printed circuit boards and found <20% variation in the slopes compared with the prior tests using an Arduino with a 5-V supply. Because this study evaluates the relative increase or decrease in a sensor's signal, the results are still valuable indicators of vehicle emissions.

This pilot demonstration included privacy protections: IRB approval (Intermountain Healthcare IRB_1051680 and University of Utah IRB_00141290), training of faculty and staff on human subjects research, and positioning the camera in a manner that made it difficult to read the license plate. However, if this type of system were deployed outside of a research setting, additional privacy measures would be needed (license plate masking and speech filtering from audio [65]).

Future work could include fixing the voltage buses on air quality node printed circuit boards, hardening the system for more extreme weather deployments, and engineering the network communication protocols to avoid radio frequency interference between the microphones and air quality nodes (shielding, filtering, or changing frequencies). We aim to investigate a machine learning algorithm that uses all available air quality measurements, particularly since CO, NO, NO_2, and VOC are more relevant to health impacts, to support idling status predictions. After these improvements, we could deploy the system in other areas with increased idling (schools). In addition, a comparison between the vehicle emissions measurements and a plume dissipation model (e.g. Gaussian plume dispersion model) would provide information to help optimize the sensor placement.

VI. Conclusion

In this study, we effectively demonstrate a novel system that can detect idling vehicles, measure vehicle emission impact on local air quality, and provide real-time feedback to drivers about idling behavior and air quality in the area. In addition, we show that this system is effective at reducing idling behavior, with an average 28.0% reduction in idling time, and thus, this reduction in idling has a measurable impact on local vehicle emissions, with a 29.5% decrease in CO_2 emissions compared with background. This novel approach to combat discretionary vehicle idling can supplement current anti-idling strategies.

Acknowledgment

The authors would like to thank the Intermountain Health and Intermountain LDS Hospital for hosting the project at the LDS Hospital Facility. They also thank to Dr. Liz Joy, M.D., M.PH., who was the Senior Medical Wellness and Nutrition Director at Intermountain Health during the project.

VIII. Conflict of Interest

Pierre-Emmanuel Gaillardon, Ross Whitaker, and Kerry Kelly have an interest in the company TELLUS Networked Sensor Solutions Inc., which commercializes solutions for environmental monitoring. No TELLUS products were used in this study.

References

[1] S. Anenberg, J. Miller, D. Henze, and R. Minjares. (2019). *A Global Snapshot of the Air Pollution-Related Health Impacts of Transportation Sector Emissions in 2010 and 2015*. International Council on Clean Transportation. [Online]. Available: https://theicct.org/wp-content/uploads/2021/06/Global_health_impacts_transport_emissions_2010-2015_20190226.pdf

[2] OECD. (Jun. 2016). *The Economic Consequences of Outdoor Air Pollution*. [Online]. Available: https://www.oecd.org/content/dam/oecd/en/publications/reports/2016/06/the-economic-consequences-of-outdoor-air-pollutiong1g68583/9789264257474-en.pdf

[3] World Bank. (Apr. 2022). *The Global Health Cost of PM2.5 Air Pollution: A Case for Action Beyond 2021*. [Online]. Available: https://documents.worldbank.org/en/publication/documents-reports/documentdetail/455211643691938459/the-global-health-cost-of-PM-2-5-air-pollution-a-case-for-action-beyond-2021

[4] R. N. Annavarapu and S. Kathi, "Cognitive disorders in children associated with urban vehicular emissions," *Environ. Pollut.*, vol. 208, pp. 74–78, Jan. 2016. [Online]. Available: https://linkinghub.elsevier.com/retrieve/pii/S0269749115300828

[5] M. B. Rice et al., "Lifetime exposure to ambient pollution and lung function in children," *Amer. J. Respiratory Crit. Care Med.*, vol. 193, no. 8, pp. 881–888, Apr. 2016. [Online]. Available: https://www.atsjournals.org/doi/10.1164/rccm.201506-1058OC

[6] T. K. M. Beatty and J. P. Shimshack, "School buses, diesel emissions, and respiratory health," *J. Health Econ.*, vol. 30, no. 5, pp. 987–999, Sep. 2011. [Online]. Available: https://linkinghub.elsevier.com/retrieve/pii/S0167629611000701

[7] H. S. Kenagy, C. Lin, H. Wu, and M. R. Heal, "Greater nitrogen dioxide concentrations at child versus adult breathing heights close to urban main road kerbside," *Air Qual., Atmos. Health*, vol. 9, no. 6, pp. 589–595, Sep. 2016. [Online]. Available: http://link.springer.com/10.1007/s11869-015-0370-3

[8] (May 2015). *Idling Reduction for Personal Vehicles*. [Online]. Available: https://afdc.energy.gov/files/u/publication/idling_personal_vehicles.pdf

[9] P. H. Ryan et al., "The impact of an anti-idling campaign on outdoor air quality at four urban schools," *Environ. Science: Processes Impacts*, vol. 15, no. 11, p. 2030, 2013. [Online]. Available: https://xlink.rsc.org/?DOI=c3em00377a

[10] M. D. Adams and W. J. Requia, "How private vehicle use increases ambient air pollution concentrations at schools during the morning drop-off of children," *Atmos. Environ.*, vol. 165, pp. 264–273, Sep. 2017. [Online]. Available: https://linkinghub.elsevier.com/retrieve/pii/S1352231017304351

[11] A. Sharma and P. Kumar, "A review of factors surrounding the air pollution exposure to in-pram babies and mitigation strategies," *Environ. Int.*, vol. 120, pp. 262–278, Nov. 2018. [Online]. Available: https://linkinghub.elsevier.com/retrieve/pii/S0160412018306585

[12] J. Dowds, J. Sullivan, and L. Aultman-Hall, "Comparisons of discretionary passenger vehicle idling behavior by season and trip stage with global positioning system and onboard diagnostic devices," *Transp. Res. Rec., J. Transp. Res. Board*, vol. 2341, no. 1, pp. 76–82, Jan. 2013. [Online]. Available: https://journals.sagepub.com/doi/10.3141/2341-08

[13] A. R. Carrico, P. Padgett, M. P. Vandenbergh, J. Gilligan, and K. A. Wallston, "Costly myths: An analysis of idling beliefs and behavior in personal motor vehicles," *Energy Policy*, vol. 37, no. 8, pp. 2881–2888, Aug. 2009. [Online]. Available: https://linkinghub.elsevier.com/retrieve/pii/S0301421509001633

[14] C. Eghbalnia et al., "A community-based participatory research partnership to reduce vehicle idling near public schools," *J. Environ. Health*, vol. 75, no. 9, pp. 14–19, May 2013. [Online]. Available: https://www.jstor.org/stable/26329619

[15] R. Meleady et al., "Surveillance or self-surveillance? Behavioral cues can increase the rate of drivers' pro-environmental behavior at a long wait stop," *Environ. Behav.*, vol. 49, no. 10, pp. 1156–1172, Dec. 2017. [Online]. Available: http://journals.sagepub.com/doi/10.1177/0013916517691324

[16] J. Van de Vyver, D. Abrams, T. Hopthrow, K. Purewal, G. R. de Moura, and R. Meleady, "Motivating the selfish to stop idling: Self-interest cues can improve environmentally relevant driver behaviour," *Transp. Res. F, Traffic Psychol. Behav.*, vol. 54, pp. 79–85, Apr. 2018. [Online]. Available: https://linkinghub.elsevier.com/retrieve/pii/S1369847817306812

[17] B. Beusen et al., "Using on-board logging devices to study the longer-term impact of an eco-driving course," *Transp. Res. D, Transp. Environ.*, vol. 14, no. 7, pp. 514–520, Oct. 2009. [Online]. Available: https://linkinghub.elsevier.com/retrieve/pii/S1361920909000698

[18] M. A. Winnett and A. H. Wheeler, "Vehicle-activated signs—A large scale evaluation," Transport Research Laboratory, Crowthorne, U.K., Tech. Rep. TRL 548, 2002. [Online]. Available: https://www.trl.co.uk/publications/trl548

[19] G. L. Ullman and E. R. Rose, "Evaluation of dynamic speed display signs," *Transp. Res. Rec., J. Transp. Res. Board*, vol. 1918, no. 1, pp. 92–97, Jan. 2005. [Online]. Available: https://journals.sagepub.com/doi/10.1177/0361198105191800112

[20] C. Lee, S. Lee, B. Choi, and Y. Oh, "Effectiveness of speed-monitoring displays in speed reduction in school zones," *Transp. Res. Rec., J. Transp. Res. Board*, vol. 1973, no. 1, pp. 27–35, Jan. 2006. [Online]. Available: https://journals.sagepub.com/doi/abs/10.1177/0361198106197300104?casa_token=ub4PiVx7l5cAAAAA:4I3poJbkTkK5dT4LHhX4_PpiBIr7sIL94B7xfJeSwWUvVKNKC5-hTMGBWB0BGJkhSa4ejF0kS7W5vSg

[21] I. Cruzado and E. T. Donnell, "Evaluating effectiveness of dynamic speed display signs in transition zones of two-lane, rural highways in Pennsylvania," *Transp. Res. Rec., J. Transp. Res. Board*, vol. 2122, no. 1, pp. 1–8, Jan. 2009. [Online]. Available: https://journals.sagepub.com/doi/10.3141/2122-01

[22] B. Schlag, J. Stern, P. Butterwegge, and S. Degener, "Evaluation of the dialog-display-Berlin studies," German Insurance Assoc. Insurers Accident Res., Berlin, Germany, Tech. Rep. VV 01, Mar. 2009.

[23] R. Ando et al., "Long-term effect analysis of dynamic speed display sign in streets," in *Proc. 4th Int. Conf. Transp. Inf. Safety (ICTIS)*, Aug. 2017, pp. 522–529. [Online]. Available: http://ieeexplore.ieee.org/document/8047815/

[24] G. A. van Kleef, F. Wanders, E. Stamkou, and A. C. Homan, "The social dynamics of breaking the rules: Antecedents and consequences of norm-violating behavior," *Current Opinion Psychol.*, vol. 6, pp. 25–31, Dec. 2015. [Online]. Available: https://linkinghub.elsevier.com/retrieve/pii/S2352250X15001189

[25] D. Abrams and M. A. Hogg, "Social identification, self-categorization and social influence," *Eur. Rev. Social Psychol.*, vol. 1, no. 1, pp. 195–228, Jan. 1990. [Online]. Available: http://www.tandfonline.com/doi/abs/10.1080/14792779108401862

[26] J. M. Bas-Hoogendam, H. van Steenbergen, T. Kreuk, N. J. A. van der Wee, and P. M. Westenberg, "How embarrassing! The behavioral and neural correlates of processing social norm violations," *PLoS ONE*, vol. 12, no. 4, Apr. 2017, Art. no. e0176326. [Online]. Available: https://dx.plos.org/10.1371/journal.pone.0176326

[27] D. J.-F. de Quervain et al., "The neural basis of altruistic punishment," *Science*, vol. 305, no. 5688, pp. 1254–1258, Aug. 2004. [Online]. Available: https://www.science.org/doi/10.1126/science.1100735

[28] E. Fehr and S. Gächter, "Altruistic punishment in humans," *Nature*, vol. 415, no. 6868, pp. 137–140, Jan. 2002. [Online]. Available: https://www.nature.com/articles/415137a

[29] C. Molho, J. M. Tybur, P. A. M. Van Lange, and D. Balliet, "Direct and indirect punishment of norm violations in daily life," *Nature Commun.*, vol. 11, no. 1, p. 3432, Jul. 2020. [Online]. Available: https://www.nature.com/articles/s41467-020-17286-2

[30] G. A. van Kleef, "Bottom-up influences on social norms: How observers' responses to transgressions drive norm maintenance versus change," *Current Opinion Psychol.*, vol. 60, Dec. 2024, Art. no. 101919. [Online]. Available: https://linkinghub.elsevier.com/retrieve/pii/S2352250X24001325

[31] S. Mahmoudi, S. Peck, K. B. Smith, K. Kelly, and G. J. Madden, "Effect of dynamic social norm messaging on intent to idle," *J. Environ. Psychol.*, vol. 105, Aug. 2025, Art. no. 102635. [Online]. Available: https://linkinghub.elsevier.com/retrieve/pii/S0272494425001185

[32] Y. Liang, D. Sengupta, M. J. Campmier, D. M. Lunderberg, J. S. Apte, and A. H. Goldstein, "Wildfire smoke impacts on indoor air quality assessed using crowdsourced data in California," *Proc. Nat. Acad. Sci. USA*, vol. 118, no. 36, Sep. 2021, pp. 1–6. [Online]. Available: https://pnas.org/doi/full/10.1073/pnas.2106478118

[33] K. E. Kelly et al., "Community-based measurements reveal unseen differences during air pollution episodes," *Environ. Sci. Technol.*, vol. 55, no. 1, pp. 120–128, Jan. 2021. [Online]. Available: https://pubs.acs.org/doi/10.1021/acs.est.0c02341

[34] A. Zafra-Pérez, J. Medina-García, C. Boente, J. A. Gómez-Galán, A. Sánchez de la Campa, and J. D. de la Rosa, "Designing a low-cost wireless sensor network for particulate matter monitoring: Implementation, calibration, and field-test," *Atmos. Pollut. Res.*, vol. 15, no. 9, Sep. 2024, Art. no. 102208. [Online]. Available: https://linkinghub.elsevier.com/retrieve/pii/S1309104224001739

[35] D. V. Mallia et al., "Evaluating wildfire smoke transport within a coupled fire-atmosphere model using a high-density observation network for an episodic smoke event along Utah's wasatch front," *J. Geophys. Res., Atmos.*, vol. 125, no. 20, p. 2020, Oct. 2020. [Online]. Available: https://agupubs.onlinelibrary.wiley.com/doi/10.1029/2020JD032712

[36] J. He, C.-H. Huang, N. Yuan, E. Austin, E. Seto, and I. Novosselov, "Network of low-cost air quality sensors for monitoring indoor, outdoor, and personal PM_2.5 exposure in Seattle during the 2020 wildfire season," *Atmos. Environ.*, vol. 285, Sep. 2022, Art. no. 119244. [Online]. Available: https://linkinghub.elsevier.com/retrieve/pii/S1352231022003090

[37] P. Kortoçi et al., "Air pollution exposure monitoring using portable low-cost air quality sensors," *Smart Health*, vol. 23, Mar. 2022, Art. no. 100241. [Online]. Available: https://linkinghub.elsevier.com/retrieve/pii/S235264832100057X

[38] P. Kumar et al., "The rise of low-cost sensing for managing air pollution in cities," *Environ. Int.*, vol. 75, pp. 199–205, Feb. 2015. [Online]. Available: https://linkinghub.elsevier.com/retrieve/pii/S0160412014003547

[39] T. Mangin et al., "Understanding the effect of outdoor pollution episodes and HVAC type on indoor air quality," *Building Environ.*, vol. 278, Jun. 2025, Art. no. 112978. [Online]. Available: https://linkinghub.elsevier.com/retrieve/pii/S0360132325004597

[40] G. Liu et al., "Cyber-physical system-based real-time monitoring and visualization of greenhouse gas emissions of prefabricated construction," *J. Cleaner Prod.*, vol. 246, Feb. 2020, Art. no. 119059. [Online]. Available: https://linkinghub.elsevier.com/retrieve/pii/S0959652619339290

[41] D. Bej and N. Chattaraj, "Air pollution from vehicle-tailpipe emissions and diagnostic approaches through cyber–physical platform—A review," *Microprocessors Microsystems*, vol. 98, Apr. 2023, Art. no. 104805. [Online]. Available: https://linkinghub.elsevier.com/retrieve/pii/S0141933123000510

[42] O. Farrag, A. Mansour, B. Abed, A. Abu Alhaj, T. Landolsi, and A. R. Al-Ali, "IVEMPS: IoT-based vehicle emission monitoring and prediction system," *IEEE Access*, vol. 13, pp. 95628–95646, 2025. [Online]. Available: https://ieeexplore.ieee.org/document/11009199/

[43] N. Sharma, M. Advani, R. Dhyani, S. Nagar, and H. Chaudhary, "Reduction in idling fuel losses and corresponding emissions due to awareness campaign at the signalized intersections in Delhi," *Transp. Developing Economies*, vol. 8, no. 1, p. 11, Apr. 2022. [Online]. Available: https://link.springer.com/10.1007/s40890-021-00146-z

[44] D. L. Mendoza et al., "Air quality and behavioral impacts of anti-idling campaigns in school drop-off zones," *Atmosphere*, vol. 13, no. 5, p. 706, Apr. 2022. [Online]. Available: https://www.mdpi.com/2073-4433/13/5/706

[45] K. Rumchev, A. Lee, B. Maycock, and J. Jancey, "Reducing car idling at primary schools: An intervention study of parent behaviour change in Perth, Western Australia," *Health Promotion J. Aust.*, vol. 32, no. 3, pp. 383–390, Jul. 2021. [Online]. Available: https://onlinelibrary.wiley.com/doi/10.1002/hpja.381

[46] D. Abrams et al., "Cleaning up our acts: Psychological interventions to reduce engine idling and improve air quality," *J. Environ. Psychol.*, vol. 74, Apr. 2021, Art. no. 101587. [Online]. Available: https://linkinghub.elsevier.com/retrieve/pii/S0272494421000402

[47] X. Li et al., "Real-time idling vehicles detection using combined audio-visual deep learning," in *Emerging Cutting-Edge Developments in Intelligent Traffic and Transportation Systems*. Amsterdam, The Netherlands: IOS Press, 2024, pp. 142–158.

[48] M. Bastan, K.-H. Yap, and L.-P. Chau, "Remote detection of idling cars using infrared imaging and deep networks," *Neural Comput. Appl.*, vol. 32, no. 8, pp. 3047–3057, Apr. 2020. [Online]. Available: http://link.springer.com/10.1007/s00521-019-04077-0

[49] Y. Ding, X. Zhao, J. Luo, G. Wu, and A. Venkatram, "Field study to estimate exposure to vehicle exhaust during idling and starting," *Atmos. Pollut. Res.*, vol. 14, no. 1, Jan. 2023, Art. no. 101632. [Online]. Available: https://linkinghub.elsevier.com/retrieve/pii/S1309104222003130

[50] R. M. Duvall et al., "Performance tesing protocols, metrics, and target values for fine particulate matter air sensors," EPA, Washington, DC, USA, Tech. Rep. 600/R-20/280, Feb. 2021.

[51] R. Duvall et al., "NO_2, CO, and SO_2 supplement to the 2021 report on performance testing protocols, metrics, and target values for ozone air sensors," EPA, Tech. Rep. EPA/600/R-23/146, Jan. 2024.

[52] J. L. Williams, C. H. Skinner, R. G. Floyd, A. D. Hale, C. Neddenriep, and E. P. Kirk, "Words correct per minute: The variance in standardized reading scores accounted for by reading speed," *Psychol. Schools*, vol. 48, no. 2, pp. 87–101, Feb. 2011. [Online]. Available: https://onlinelibrary.wiley.com/doi/10.1002/pits.20527

[53] F. R. Valverde, J. V. Hurtado, and A. Valada, "There is more than meets the eye: Self-supervised multi-object detection and tracking with sound by distilling multimodal knowledge," in *Proc. IEEE/CVF Conf. Comput. Vis. Pattern Recognit. (CVPR)*, Jun. 2021, pp. 11607–11616. [Online]. Available: https://api.semanticscholar.org/CorpusID:232092247

[54] *Local Climatological Data Station Details*. Accessed: Feb. 3, 2025. [Online]. Available: https://www.ncei.noaa.gov/cdo-web/datasets/LCD/stations/WBAN:24127/detail

[55] R. B. Cialdini, R. R. Reno, and C. A. Kallgren, "A focus theory of normative conduct: Recycling the concept of norms to reduce littering in public places," *J. Personality Social Psychol.*, vol. 58, no. 6, pp. 1015–1026, Jun. 1990, doi: 10.1037/0022-3514.58.6.1015.

[56] D. Abrams and M. A. Hogg, *Social Identity Theory: Constructive and Critical Advances*. Cham, Switzerland: Springer, 1990. [Online]. Available: https://psycnet.apa.org/record/1990-98968-000

[57] R. M. Kudela, S. B. Hooker, L. S. Guild, H. F. Houskeeper, and N. Taylor, "Expanded signal to noise ratio estimates for validating next-generation satellite sensors in oceanic, coastal, and inland waters," *Remote Sens.*, vol. 16, no. 7, p. 1238, Mar. 2024. [Online]. Available: https://www.mdpi.com/2072-4292/16/7/1238

[58] (Aug. 2019). *Signal to Noise Ratio*. [Online]. Available: https://www.itl.nist.gov/div898/software/dataplot/refman2/auxillar/snr.htm

[59] "1.3.5.17. Detection of outliers," in *E-Handbook of Statistical Methods*. NIST/SEMATACH, Apr. 2012. [Online]. Available: https://www.itl.nist.gov/div898/handbook/eda/section3/eda35h.htm

[60] A. Falk, E. Fehr, and U. Fischbacher, "Driving forces behind informal sanctions," *Econometrica*, vol. 73, no. 6, pp. 2017–2030, Nov. 2005, doi: 10.1111/j.1468-0262.2005.00644.x. [Online]. Available: http://doi.wiley.com/10.1111/j.1468-0262.2005.00644.x

[61] B. Armstrong and M. Montagnese. (2009). *'Turn It Off' Anti-Idling Campaign Report, Simcoe Muskoka District Health Unit*. [Online]. Available: https://www.simcoemuskokahealth.org/docs/default-source/jfy-communities/tio simcoe-muskoka report final public

[62] F. Karagulian et al., "Review of the performance of low-cost sensors for air quality monitoring," *Atmosphere*, vol. 10, no. 9, p. 506, Aug. 2019. [Online]. Available: https://www.mdpi.com/2073-4433/10/9/506

[63] Y. Wang et al., "Quantitative study of vehicle CO_2 emission at various temperatures and road loads," *Fuel*, vol. 320, Jul. 2022, Art. no. 123911. [Online]. Available: https://linkinghub.elsevier.com/retrieve/pii/S0016236122007700

[64] Senseair. (2019). *Product Specification K30 FR Fast Response CO_2 Sensor, PSP0109*. [Online]. Available: chrome-extension://efaidnbmnnnibpcajpcglclefindmkaj/https://rmtplusstoragesenseair.blob.core.windows.net/docs/publicerat/PSP109.pdf

[65] S. Boovaraghavan, H. Zhou, M. Goel, and Y. Agarwal, "Kirigami: Lightweight speech filtering for privacy-preserving activity recognition using audio," *Proc. ACM Interact., Mobile, Wearable, Ubiquitous Technol.*, vol. 8, no. 1, pp. 1–28, 2024.

Tristalee Mangin received the B.S. degree in chemical engineering from The University of Utah, Salt Lake City, UT, USA, in 2014, where she is currently pursuing the Ph.D. degree in chemical engineering.

Her research focuses on low-cost sensor applications, with an emphasis on data quality and data science, and the development and evaluation of IoT-based air quality solutions.

Xiwen Li is currently pursuing the Ph.D. degree in computer science with The University of Utah, Salt Lake City, UT, USA.

His research focuses on the application of deep learning algorithms to challenges in computer vision, audio signal processing, and audio–video fusion.

Saba Mahmoudi is currently pursuing the Ph.D. degree in psychology program with The Utah State University, Salt Lake City, UT, USA, specializing in behavior analysis.

Her research interests include delay discounting and reducing impulsive choices to prevent severe problem behavior and promote healthy decision-making.

Rehman Mohammed received the M.S. degree in computer science from The University of Utah, Salt Lake City, UT, USA, in 2024.

His research focuses on image processing, computer vision, and medical image analysis.

Nathan Page received the B.S. degree in computer engineering and the M.S. degree in electrical and computer engineering from The University of Utah, Salt Lake City, UT, USA, in 2021.

He currently works as a Senior Software Engineer with TELLUS Networked Sensor Solutions, Salt Lake City. His work focused on machine learning and embedded systems.

Sara Peck received the Ph.D. degree in psychology from Utah State University, Salt Lake City, UT, USA, in 2022.

She is currently a Board Certified Behavior Analyst-Doctoral (BCBA-D) and a Faculty Member with Western New England University, Springfield, MA, USA. Her primary area of research involves interventions to promote adaptive decision-making and translation of those interventions to clinical populations, problems, and settings.

Ashton Snelgrove (Senior Member, IEEE) received the B.S. degree in computer science and the M.S. degree in computer engineering from The University of Utah, Salt Lake City, UT, USA, in 2012 and 2024, respectively, where he is currently pursuing the Ph.D. degree in electrical and computer engineering.

His research focuses on the application of design automation techniques and concepts to the design of microfluidic devices.

Evan Blanchard received the B.S. degree in chemical engineering from The University of Utah, Salt Lake City, UT, USA, in 2025.

Dillon Tang received the B.S. degree in chemical engineering from The University of Utah, Salt Lake City, UT, USA, in 2025.

Lizzie Pinegar received the B.S. degree in chemical engineering and atmospheric science from The University of Utah, Salt Lake City, UT, USA, in 2024.

Owen Leishman received the B.S. degree from the Department of Electrical Engineering, The University of Utah, Salt Lake City, UT, USA, in 2024.

J. Nicholas Rice received the M.S. degree in industrial hygiene and occupational health from the School of Medicine, University of Utah, Salt Lake City, UT, USA, in 2013.

He is a CIH and a CSP and serves as the Enterprise Safety and Industrial Hygiene Director at Intermountain Health. His work focuses on environmental health, exposure science, indoor air quality, and occupational injury prevention.

Gregory Madden is currently a Professor with the Department of Psychology, The Utah State University, Salt Lake City, UT, USA. He specializes in behavioral economics and impulsive decision-making.

Pierre-Emmanuel Gaillardon (Senior Member, IEEE) is currently a Professor and an Associate Chair with the Department of Electrical and Computer Engineering (ECE) and an Adjunct Faculty with the Kahlert School of Computing, The University of Utah, Salt Lake City, UT, USA, where he leads the Laboratory for NanoIntegrated Systems (LNIS).

Prof. Gaillardon was a recipient of numerous awards, including the NSF CAREER Award, the DARPA Young Faculty Award, and the DAC under-40 Innovators Award.

Ross Whitaker is currently a Professor Emeritus with the Kahlert School of Computing, The University of Utah, Salt Lake City, UT, USA.

Kerry Kelly is currently an Associate Professor of chemical engineering with The University of Utah, Salt Lake City, UT, USA. She also focuses on the translation of science into policy through service on Utah's Air Quality Board and on Utah's Air Quality Policy Board. Her research focuses on using cost-effective sensing to understand and address local and regional air quality challenges.